

Interactions between vegetation, sedimentation and flood inundation levels in wetlands

Marianna Soler^{a,*}, Jordi Colomer^a, Andrew Folkard^b, Teresa Serra^a

^a Department of Physics, University of Girona, Universitat de Girona, 4, Campus Montilivi, 17003, Girona, Spain

^b Lancaster Environment Centre, Lancaster University, Lancaster, LA1 4YQ, United Kingdom

ARTICLE INFO

Keywords:

Peak flow hydrodynamic regimes
Laboratory flume experiments
Natural vegetation
Sedimentation patterns

ABSTRACT

Wetlands produce key ecosystem services to mitigate the impacts of peak flows caused by pluvial or fluvial floods or storm surges. Sediment floods were characterized by a peak flow flowing over a simulated wetland, populated with two natural species. Floods have been drawn as flows of height H , into waters of height h , where $H > h$. Peak flow along the flume passed through: peak flow adjustment; peak flow; drag-dominated peak flow; and gravity current regimes. For high inundation wetland levels, settling rates of coarse and fine sediment were similar during the peak flow regime. At larger distances, sedimentation decreased monotonically, with higher sedimentation of fine particles. For low inundation levels, the sedimentation rate during the drag-dominated peak flow regime was higher for coarse particles. Vegetation decreased the inundation level needed for enhancing sedimentation. Our study then adds practical knowledge at considering that the synergies between the vegetation and the inundation level may enhance wetland services such as the mitigation of pluvial, fluvial or coastal floodings.

1. Introduction

Wetlands are very productive environments with high levels of biodiversity providing habitat for a wide variety of species, many of which are exclusive to these environments (Balwan and Kour, 2021; Larson and Adamus, 1989). They also serve as coastal protection structures via hydrological and biogeochemical processes (Junk et al., 2013), contributing to their protection against floods, preventing soil erosion (Barcelona et al., 2018; Lo et al., 2017), promoting sedimentation and soil stabilization (Montakhab et al., 2012), and maintaining water quality through retention, removal and transformation of nutrients. In addition, wetlands contribute to the mitigation of climate change, since they are carbon sinks, holding between 20 and 30% of the Earth's total soil carbon (Nahlik and Fennessy, 2016) and reduce the consequences of the increased frequency and intensity of extreme weather phenomena (Fairchild et al., 2021; Jones et al., 2020).

Wetlands are globally subject to anthropogenic impacts that harm their conservation, cause their regression and, in extreme cases, lead to their disappearance (Gardner and Finlayson, 2018). These impacts are caused by the drainage and conversion of the land for agricultural activities (Luo et al., 2022), the expansion of urbanization and tourist

development (Chen et al., 2023), water pollution (Fu et al., 2023), and the introduction of invasive species (Choi et al., 2021; Shin et al., 2022). Climate change also represents a threat to the future of coastal wetlands (Duarte, 2002; Marbà and Duarte, 2010), especially due to water scarcity and society pressures (Lefebvre et al., 2019) with society development in coastline areas exacerbating water stress (Davidson, 2014).

The increase in global warming will impact coastal areas with an increase in sea level and erosive processes (Gedan et al., 2009; Reed et al., 2018), and an increase in the frequency of hydrometeorological phenomena such as coastal flooding and maritime storms (Hoggart et al., 2014). Inland wetlands are also to be increasingly affected by pluvial and fluvial floods (Kundzewicz and Pinskiwar, 2022).

Floods in wetlands can be caused by the effect of extreme rainfalls in rivers or by the effect of storms in coastal areas. When there is a high rainfall intensity in a short period of time that exceeds the capacity of infiltration it can result in a pluvial inundation (Sauer, J., 2022) or if water level rise exceeding the riverbank it can result in a fluvial inundation. Sometimes, coastal wetlands are inundated by the abnormal rise in seawater level during a storm (Storm surge) (Wamsley et al., 2010). In other occasions, several hydrological processes combine leading to a complex pattern in the flooding level of the saltmarsh area,

* Corresponding author. c/ Universitat de Girona, 4 Campus Montilivi, 17003 Girona, Spain.

E-mail addresses: marianna.soler@udg.edu (M. Soler), jordi.colomer@udg.edu (J. Colomer), a.folkard@lancaster.ac.uk (A. Folkard), teresa.serra@udg.edu (T. Serra).

compromising also the future of the ecosystem (McGrath et al., 2023). All these inundation processes are of concern to riparian and coastal communities and can result in increased runoff rates, volumes and peak flows which can be reduced by wetland ecosystems helping therefore to decrease the impact of downstream flooding (Babbar-Sebens et al., 2013; Lemke and Richmond, 2009; Mitsch and Day, 2006).

Vegetation in wetlands helps reduce the speed of floods as they flow over the landscape, and they can also provide immense water storage benefits while slowing water circulation to further reduce the height of floods and associated erosion rates (Healey et al., 2023; Sheng et al., 2022). When plant density, frontal area and stiffness increase, it results in a reduction of mean flow speed (Kadlec 1990; Västilä and Järvelä, 2014), resulting in both the enhancement of sediment deposition (Soler et al., 2017) along with a reduction of sediment resuspension (Leonard and Luther 1995; Ward et al., 1984). In degraded wetlands with less vegetation, there would be less protection against erosion therefore less sedimentation is expected to occur (Bouma et al., 2009), which would worsen the state of the soil in the wetland and would further hinder the growth of the vegetation itself. Wetlands provide immense water storage benefits while slowing water circulation to further reduce the height of floods and associated erosion rates (Healey et al., 2023; Sheng et al., 2022). Wetlands are also threatened by the effect of urban projects. Rojas et al. (2022) analyzed the flood mitigation ecosystem service of a coastal wetland in central Chile. They found that the occupation of wetland areas in central Chile is nearly a 50% projected to further rise, therefore decreasing any potential role in the flood mitigation. Flood hazard maps, for an extreme return period (500 years), show that the water volume stored by a wetland would decrease by more than 38% and the flooded area of the wetland by 30% (Rojas et al., 2022). It is then important to restore wetlands and flood plains (Brémond et al., 2013) as a policy during flood risk management (Ferreira et al., 2023). Wetlands restoration, through planting or seeding has had significantly improvement on attenuating floods peaks (Dakhalla and Parajuli, 2016; Faulkner et al., 2011). The protecting of existing wetlands has been found to provide the highest return on social investment (Pattison-Williams et al., 2018).

Considering that extreme climatic events such as drought, flooding and storms are expected to occur more frequently worldwide due to ongoing climate change, and given that wetlands play an important role in flood abatement (Acreman and Holden, 2013), soaking up and storing floodwater (Jessop et al., 2015), it is of great interest to study how wetlands can help to mitigate the impacts of peak flows caused by pluvial or fluvial floods or storm surges. This issue is addressed in the present study by performing laboratory flume peak flow experiments to simulate flood processes with the objectives of 1) studying the effects of different levels of inundation in inundated wetlands on the hydrodynamics and the associated sediment transport of a peak flow; and 2) studying the effect of vegetation in modifying the development of a peak flow and the impact in the sedimentation along the flooding development. It is generally acknowledged that wetlands have the potential to reduce flooding effects, but the magnitude of attenuation is the subject of debate and difficult to assess. The present study is focused on study the effect of peak flows in flooded wetlands with an experimental inundated vegetated area of height h receiving a peak flow of height H . The experiments carried out in this study, where $H > h$, complementing those where $H = h$ concerning gravity sediment-laden currents previously reported largely in the literature (Soler et al., 2020, 2021), and those where $h = 0$ corresponding to peak flows in dry wetlands (Hooke, 2019; Laronne and Reid, 1993).

This paper adds knowledge on the impacts of both the wetland inundation level and the vegetation water resistance on hydrodynamics and sedimentary patterns in front of a peak flow. This represents an advancement over previous studies of wetland benefits in front of flooding events and can provide management strategies of natural wetlands (Ferreira et al., 2023) or even a better optimisation of wetlands designed for natural based solutions in order to minimize the peak floods events.

2. Methodology

2.1. Experimental setup

Experiments were conducted in a 4.40 m long, 0.30 m high and 0.30 m wide methacrylate flume that was separated into two sections by a removable vertical lock gate. The shorter section (to the left in Fig. 1A), of 1.25 m length, acted as a reservoir containing sediment-laden water that would form the peak flow. The longer section (to the right in Fig. 1A) of 3.15 m length simulated the flooded environment where the interaction of the peak flow with the vegetation occurred. The initial water height, H , in the shorter section ranged from 25% to 50% of the canopy plants height, i.e. 6–12 cm and with an initial volume V_0 (see Table 1). The initial height of the longer section where the peak flow developed, h , ranged from 12.5% to 37.5% of the canopy plants height, i.e. 3 and 9 cm (Table 1). These inundation levels are in the range of those observed in natural wetlands of 5%–50 % (Casanova and Brock, 2000). The height of the wall at the end of the long section was modified in each experiment by taking the height h of the flooded area in order to avoid the reflection of the flood wave. The various combinations of these heights resulted in eighteen experimental runs. In twelve runs the peak flow developed in a vegetated section where after the peak flow event canopy was submerged always less than 50% of its plants height (in vegetated runs) and in the other six runs, it developed in a section without vegetation. Across the whole experiment, the variable $H-h$ ranged between 3 and 9 cm, with the height h ranging from 3 to 9 cm, in order to simulate low to high inundation levels. Condition $H-h = 0$ (i.e. $H = h$) was not considered since it would correspond to a gravity current, already studied (Soler et al., 2017, 2020, 2021), and corresponding to a different hydrodynamical process from a peak flow. Runs started once the lock gate was lifted and finished when the peak flow arrived at the end of the flume. In order to test for replicability, Run #5 (Table 1) was repeated 3 times.

2.2. Wetland vegetation characteristics

The vegetation was positioned in the longer section of the flume (right hand side in Fig. 1). Two species of natural vegetation were used: *Arthrocnemum fruticosum* and *Juncus maritimus*, both of which are native to Mediterranean salt marsh areas in marine inter-tidal environments and common in temperate climatic zones. Both species are characteristic of either inundated or non-inundated coastal wetlands (Batriu et al., 2011), reaching heights of 50–100 cm.

Plant individuals were collected from field sites in the Empordà marshes Natural Park (La Pletera), NE Spain. Sample plants with unusually high or low turgidity (judged subjectively) were not selected to maintain a standard set of plant characteristics. The plants within the vegetated section were randomly distributed by means of a random number generator, following Pujol et al. (2013). Plant density was quantified, following Pujol et al. (2010) using the solid plant fraction (SPF), which is defined as the fractional area at the bed occupied by the vegetation stems, $SPF = 100 N\pi(d/2)^2/A$, where N is the total number of plants, A is the total bed area and d is the diameter of the plant stem. For all experiments with vegetation (experiments 1 to 12 in Table 1) a constant SPF of 1.0% was used (Fig. 1B.3), corresponding to a canopy density of 356 obstacles m^{-2} , which is characteristic of coastal intertidal areas (Leonard and Luther, 1995).

The two types of vegetation presented different vertical distributions of frontal area for the same canopy density. *J. maritimus* is a rigid emergent plant with a slight vertical variation in its stem diameter (Fig. 1B.1). *A. fruticosum* is a rigid and emergent plant, which branches out over its height, each branch having leaves (Fig. 1B.2), resulting in wide vertical variation of its effective diameter. In order to quantify the frontal obstruction by each plant species, the vertical averaged plant diameter was determined following the method described by Soler et al. (2020). The mean diameter d for the stems of *A. fruticosum* and

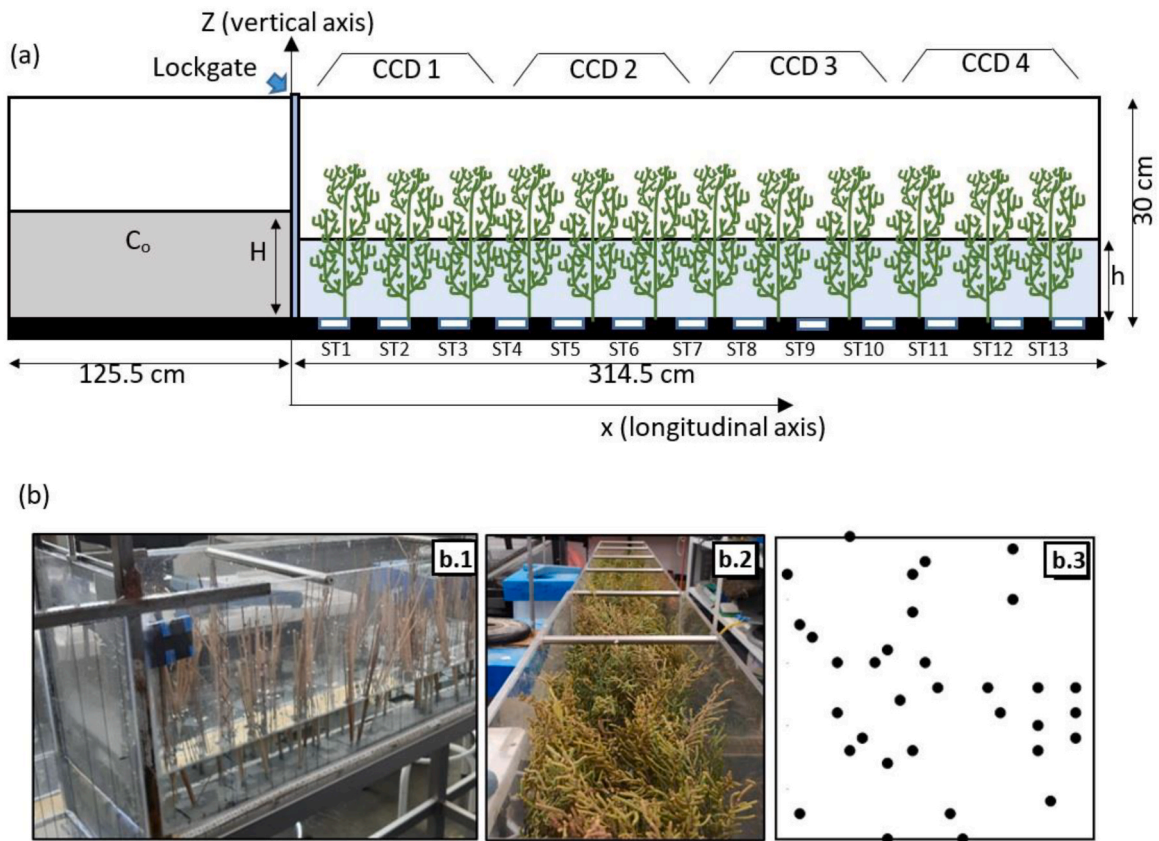


Fig. 1. a) Side view of the laboratory flume, which is divided prior to the start of each experimental run by a removable, sealing partition (lock gate) into two sections. The smaller, left-hand, section is a reservoir for preparation of the turbidity current fluid. The right-hand section contains the real or simulated vegetation and is the experimental test section. Water depth in left-hand section is H , and in right-hand section is h . The vertical coordinate is z , with $z = 0$ at the bed (increasing upwards); the longitudinal coordinate is x , with $x = 0$ at the lock gate (increasing to the right). Thirteen sediment traps (ST1 to ST13) on the flume bed. b) Images of samples of natural vegetation utilised in the experiments: (a) *Juncus maritimus* and (b) *Arthrocnemum fruticosum*. (c) Top view of the randomly-distributed array of obstacles used, with solid plant fraction (SPF) of 1.0%.

Table 1
List of experimental runs for vegetated and non-vegetated conditions for different H (initial height) and h (inundated canopy height).

Run	Vegetation	H (cm)	h (cm)
1	<i>J. maritimus</i> (SPF 1%)	12	3
2			6
3			9
4	<i>A. fruticosum</i> (SPF 1%)	9	3
5			6
6			3
7	12	3	6
8			9
9			6
10	9	3	6
11			3
12			6
13	Non-vegetated	12	3
14			6
15			9
16	9	3	6
17			6
18			3

J. Maritimus was found to be 1.6 ± 0.1 cm and 1.1 ± 0.1 cm, respectively. Data obtained for the vertical averaged diameter of the stems of *A. fruticosum* were compared with those of *J. maritimus*. For their comparison, a one-factor ANOVA was performed and significant differences between them were found ($F = 37.52$; p -value < 0.01), see Fig. 2.

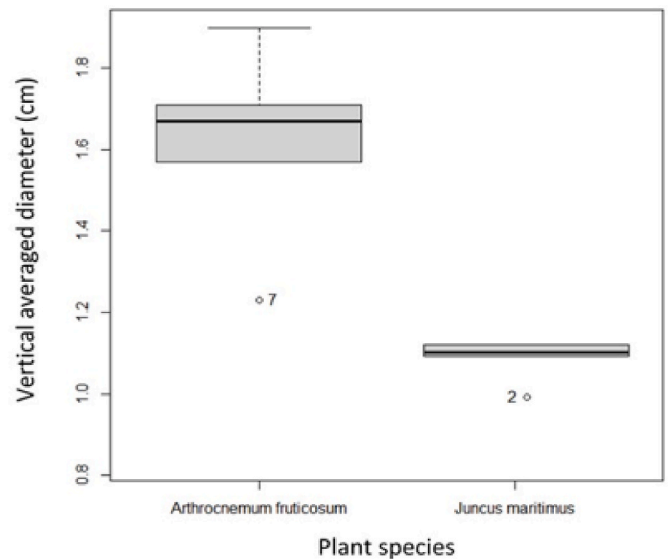


Fig. 2. Analysis one-factor ANOVA of the vertical plant diameter (d_z) values for each of the natural vegetation canopies: *Arthrocnemum fruticosum* at the left, and *Juncus maritimus* at the right. Significant differences between them were found (F -value = 37.52, p -value < 0.01).

The vertical averaged stem diameter of each individual plant, d , and the value of the frontal area of obstacles per unit volume ($a = Nd/A$, where A is the vegetated area covered with N plant shoots) (Nepf, 1999) were combined to calculate the dimensionless array density, ad . This represents the volume of the vegetated area as a proportion of the total volume of the system, and was used as a single parameter to characterize the volumetric density of the vegetation. For the experimental runs with vegetation, ad varied between 0.043 and 0.093, thus falling within the range observed in natural vegetation canopies (0.01–0.1, Kadlec, 1990; Soler et al., 2021).

2.3. Sediment characteristics and measurements

Thirteen square holes of 5 cm × 5 cm were created in the centre of the PVC base along the main axis of the flume to allocate sediment traps with the same size. The 13 traps (ST1 to ST13 in Fig. 1A) were placed in these holes (being the same height as the base sheet, thus reducing their presence in the system) within the longer section of the flume, which were 15 cm from each other. When the flood arrived at the far end of the flume, the experimental run was deemed to have ended and the traps were covered with lids to collect the deposited sediment, and avoid any additional sediment being deposited by the reflected floodwater.

The simulation of a sediment-laden peak flow consisted of a homogeneous mixture of 3 g/L of natural sediment in water, similar to that used for simulating sediment-laden gravity currents in lock gate experiments by Soler et al. (2020). The sediment used was taken from the Baix Empordà wetlands (La Pletera, NE Catalonia, Spain). Fragments of vegetation were removed from the sediment, which was then sieved to remove particles with diameter >500 μm (see the Supplementary Material for the details of the sediment). A homogeneous mixture of initial concentration $C_0 = 3$ g/L of sediment was used for section A. For this, a sediment mixture (134.54 g of sediment) was prepared in a beaker (with 3 L of water taken from section A) and strongly stirred for a minimum of 5 min. After this time, the volume of water and sediment was returned back into section A of the flume (Fig. 1A). Once the sediment was well mixed in the compartment, 10 s passed before the vertical lock gate was lifted, and the experimental run started.

The depositional flux (DF) at each sediment trap for both fine and coarse sediment particles was calculated as the deposited mass per unit area and time over which the deposition occurred. The area considered was that of the sediment trap. The depositional flux (in $\text{g cm}^{-2} \text{h}^{-1}$) was normalized by the initial horizontal flux of sediment carried by the current as it emerged from the reservoir ($C_0 v_0$), giving a non-dimensional depositional flux rate for each trap.

2.4. Determination of flood hydrodynamics

Four stationary tripods were distributed along the experimental channel on which CCD cameras were mounted to record the experiments (Fig. 1A). The cameras were used to measure the horizontal evolution of the front of the peak flow (interface between the turbid flow and clean water) along the flume over time. The mean position of the peak flow front across the transversal axis of the flume was considered to determine its temporal evolution along the main axis. Parallax error was less than 4% in these images and was not corrected for in the analysis. The horizontal position of the peak flow front was monitored at time intervals of 0.2 s along the full development of the peak flow front.

In this study, the water height difference ($H-h$), reduced gravity (g') and time (t) were considered to be the main parameters to describe the behaviour of the peak flow. The reduced gravity is $g' = g \cdot (\rho - \rho_0) / \rho_0$, where g is the gravitational acceleration and ρ and ρ_0 are the densities of the sediment and water, respectively. For the early development of the peak flow in the non-vegetated experiments, the along-flume horizontal displacement (x) of the peak flow front is expected to depend on the dimensionless parameter $(g' \cdot t^2 / (H-h))$, that is the ratio of the gravitational inertia ($g' \cdot t^2$) and the potential inertia. For the vegetated

experiments, the porosity of the vegetated zone (1- ad) was also considered.

At the final stages of the peak flow process, when the water level became even all along the flume, the flow effectively became a gravity current. Thereafter, the governing parameter that drove the front evolution was the density difference between the front (with suspended particles) and the surrounding (clear) water. As found by Soler et al. (2017, 2020), a gravity current flowing along a flume passes through three regimes (inertial, drag and viscous regimes). The inertial regime, when position of the front, x_c , varies in direct proportion to time, $x_c \propto t^1$, and depends on the reduced gravity and water depth (Tanino et al., 2005). When the gravity current is affected by the drag due to the vegetation, the temporal evolution of the front is $x_c \propto t^{1/2}$ (Hatcher et al., 2000). And when viscosity dominates the gravity current development (viscous regime), the temporal evolution of the gravity current varies as $x_c \sim t^{1/5}$.

3. Results

3.1. Hydrodynamics of the peak flow

The temporal evolution of the position of the peak flow front along the flume was analyzed to determine its relationship to the main parameters driving its behaviour. Different hydrodynamic regimes were observed.

3.1.1. Peak flow-adjustment regime

The initial phase of the peak flow ($x < 9.5(H-h)$) was identified as the peak flow-adjustment regime. For all the experimental runs, both with and without vegetation, the non-dimensional position of the peak flow, $x/(H-h)$, was found to have a statistically significant linear relationship ($r^2 = 0.85$; $n = 84$; $p < 0.05$) with $g' \cdot t^2 / (H-h)$, Fig. 3, following

$$\frac{x}{H-h} = 13.04 \cdot \left(\frac{g' \cdot t^2}{H-h} \right)^{1/2} \quad (1)$$

From equation (1), the position of the peak flow front followed:

$$x = 13.04 \cdot [g' \cdot (H-h)]^{1/2} \cdot t, \quad (2)$$

and the velocity of the peak flow front during the flow adjustment, v_{PFA} ,

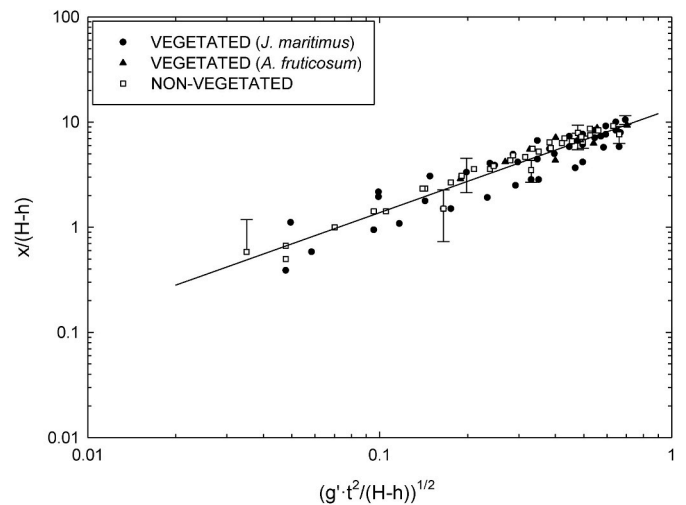


Fig. 3. Evolution, during the Peak flow-adjustment regime, of the dimensionless length ($x_c/(H-h)$) of the peak flow front versus the non-dimensional time $(g' \cdot t^2 / (H-h))^{1/2}$ for all runs: vegetated (*Juncus maritimus* (black circles), *Arthrocnemum fruticosum* (black triangles) and non-vegetated (white squares)). Line represents the linear best fit of data ($m = 13.04$; $r^2 = 0.85$; $n = 84$; $p < 0.05$).

followed

$$v_{PFA} = 13.04 \cdot [g' \cdot (H - h)]^{\frac{1}{2}} \quad (3)$$

Thus, v_{PFA} was found to be constant with time during this regime and dependent on g' and $(H-h)$.

3.1.2. Peak flow regime

For distances $9.5(H-h) < x < 27(H-h)$, the flow transitioned to a fully developed peak flow. In this regime, the peak flow behaviour depended on whether it developed in vegetated or non-vegetated beds.

In non-vegetated beds, the temporal evolution of the position of the peak flow front scaled as (see Fig. 4A):

$$\frac{x}{H-h} = 14.70 \cdot \left(\frac{g' \cdot t^2}{H-h} \right)^a \quad (4)$$

($r^2 = 0.89$; $n = 105$; $p < 0.05$), where $a = 1/2$, which follows the same temporal evolution as for the flow adjustment regime. In this case, the velocity of the peak flow, v_{PF} , was found to be constant with time and to depend on g' and $(H-h)$ according to:

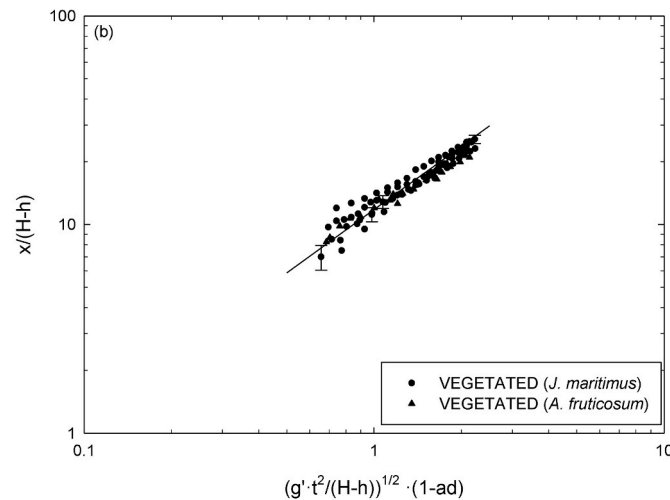
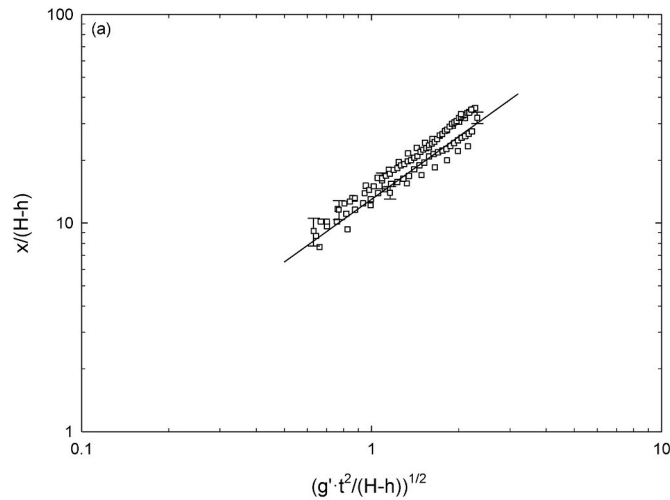


Fig. 4. Evolution, during the Fully developed peak flow regime, of the dimensionless length ($x_c/(H-h)$) of the peak flow front versus (a) the non-dimensional time $(g' \cdot t^2/(H-h))^{1/2}$ in non-vegetated runs, and (b) the non-dimensional time $(g' \cdot t^2/(H-h))^{1/2} \cdot (1-ad)$ in runs with all canopies (*Juncus maritimus* (black circles) and *Arthrocnemum fruticosum* (black triangles)). Lines represents the linear best fit of data for both the non-vegetated runs ($m = 14.70$; $r^2 = 0.89$; $n = 105$; p -value < 0.05) and the vegetated experiments ($m = 10.06$; $r^2 = 0.94$; $n = 106$; p -value < 0.05).

$$v_{PF} = 14.70 \cdot [g' \cdot (H - h)]^{\frac{1}{2}} \quad (5)$$

In contrast, in the vegetated beds, the drag exerted by the vegetation slowed the peak flow front's temporal evolution along the flume within the vegetation in a manner dependent on the non-dimensional ratio $(\frac{g' \cdot t^2}{H-h})$ and the dimensionless porosity of the vegetation $(1-ad)$. The dependence of $x/(H-h)$ on both these parameters was found empirically to follow (Fig. 4B)

$$\frac{x}{H-h} = 10.06 \cdot \left(\frac{g' \cdot t^2}{H-h} \right)^b \cdot (1-ad)^c \quad (6)$$

($r^2 = 0.94$; $n = 106$; $p < 0.05$), where $b = 1/2$ and $c = 1$. Consequently, the velocity of the peak flow in the vegetated beds during this regime, v_{PFV} , was found to follow:

$$v_{PFV} = 10.06 \cdot [g' \cdot (H - h)]^{\frac{1}{2}} \cdot (1-ad) \quad (7)$$

Therefore, like v_{FA} and v_{PF} , v_{PFV} also remained constant with time and varied with g' , $(H-h)$ and $(1-ad)$.

3.1.3. Peak flow drag dominated regime

For distances, $27 \cdot (H-h) < x < 32 \cdot (H-h)$, the vegetation played a greater role and the temporal evolution of the peak flow depended not only on the vegetation porosity $(1-ad)$ but also on the drag coefficient of the randomly-distributed array. $C_{Da} = C_D / \{1.16 [1.16 - 9.31(ad) + 38.6(ad)^2 - 59.8(ad)^3]\}$ is the drag coefficient (Ghisalberti and Nepf, 2004), where C_D is the drag coefficient for smooth isolated circular cylinders (or stems), which is a function of the stem Reynolds number, Re , such that $C_D = 1 + 10Re^{-2/3}$ (White, 1991). This regime is named the peak flow drag dominated regime. Within this regime, the evolution of the peak flow front (Fig. 5) was found to follow

$$\frac{x}{H-h} = 13.08 \cdot \left(\frac{g' \cdot t^2}{H-h} \right)^d \cdot (C_{Da}(1-ad))^e \quad (8)$$

($r^2 = 0.60$; $n = 56$; $p < 0.05$), where $d = 0.30$ and $e = 0.22$. Therefore, the velocity, v_{PFD} , of the peak flow followed:

$$v_{PFD} = 7.85 \cdot (g')^{0.3} \cdot (H-h)^{0.70} \cdot (C_{Da}(1-ad))^{0.22} \cdot t^{-2/5} \quad (9)$$

Thus, in this regime, the peak flow velocity v_{PFD} varied not only with

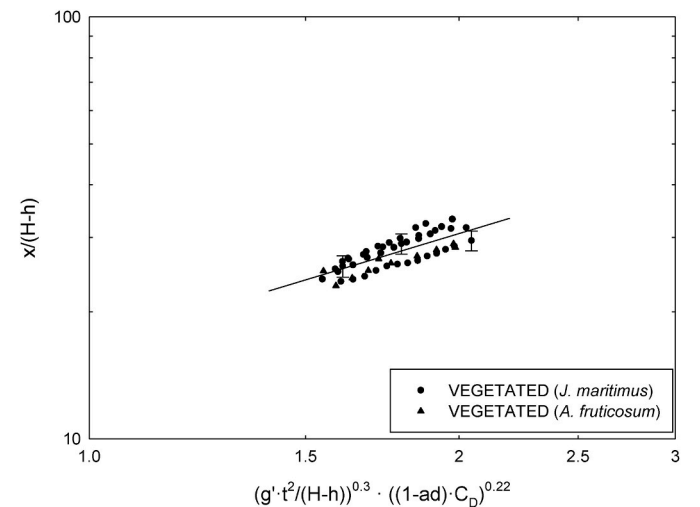


Fig. 5. Evolution, during the peak flow drag dominated regime, of the dimensionless length ($x_c/(H-h)$) of the peak flow front versus the non-dimensional time $(g' \cdot t^2/(H-h))^{0.3} \cdot ((1-ad) \cdot C_D)^{0.22}$ in runs with all canopies (*Juncus maritimus* (black circles) and *Arthrocnemum fruticosum* (black triangles)). Line represents the linear best fit of data for both the non-vegetated runs ($m = 13.08$; $r^2 = 0.60$; $n = 56$; p -value < 0.05).

g' , $(H-h)$, $(1-ad)$ and C_{D_a} but also with time.

3.1.4. Gravity current drag dominated regime and viscosity regime

For experiments with $H-h \leq 6$, and for distances $x > 32(H-h)$, the peak flow effectively became a gravity current, and in this form first flowed through a drag-dominated gravity current regime where $x \sim t^{1/2}$, and undergoing afterwards into a viscous regime of a gravity current where the front propagates as $x \sim t^{1/5}$ (see Methods section 2.4).

3.2. Sediment deposition fluxes in a peak flow event

For the non-vegetated runs, the non-dimensional deposition flux rates for both fine (Fig. 6A) and coarse particles (Fig. 6B), $DF/(C_0 \cdot v_0)$ (where C_0 was the initial sediment concentration (3 g L^{-1}) and v_0 was the initial front velocity) was plotted against the non-dimensional distance, $x/(H-h)$. For the low inundation cases ($H-h = 9 \text{ cm}$), the non-dimensional depositional flux during the initial stages in the peak flow adjustment regime and the peak flow regime was constant, and reached its maximum at the end of the peak flow regime, with $DF/(C_0 \cdot v_0) \sim 10^{-5}$ and $\sim 3 \times 10^{-5}$ for fine particles and coarse particles, respectively, at horizontal distances of $x/(H-h) \sim 30$. For moderate to high inundation cases ($H-h = 3$ and 6 cm), the behaviour of $DF/(C_0 \cdot v_0)$ with $x/(H-h)$ depended on the inundation level for both fine and coarse particles. For instance, in the highest inundated case considered ($H-h = 3 \text{ cm}$), the non-dimensional depositional flux $DF/(C_0 \cdot v_0)$ for both fine and coarse particles decreased with $x/(H-h)$, while for the intermediate inundation level of $H-h = 6 \text{ cm}$, especially for the coarse fraction, the non-dimensional depositional flux was found to increase until the transition between the peak flow and gravity current regimes, as found for the low inundation regime of $H-h = 9 \text{ cm}$.

For the vegetated runs and in low inundation experiments ($H-h = 9$

cm), $DF/(C_0 \cdot v_0)$ behaved similarly to the non-vegetated runs for both types of plant. In this case, the sedimentation rate was constant at the initial stage of the front development and reached a maximum value of $\sim 4 \times 10^{-6}$ and $\sim 4 \times 10^{-5}$ for fine particles (Fig. 6C) and coarse particles (Fig. 6D), respectively, within the peak flow drag dominated regime. In contrast, the sedimentation rates ($DF/(C_0 \cdot v_0)$) for moderate to high inundation vegetated experiments ($H-h = 6$ and 3 cm) remained nearly constant until the end of the peak flow regime. After that, $DF/(C_0 \cdot v_0)$ decreased to the end of the flume, within the gravity current regime. In the gravity current regime, $DF/(C_0 \cdot v_0)$ for fine particles was independent of the vegetation type, whereas for coarse particles it was nearly 3 times greater in runs with *J. maritimus* than in those with *A. fruticosum*.

In order to study the effect of vegetation and the level of inundation on the transport of sediments, the non-dimensional depositional flux $DF/(C_0 \cdot v_0)$ was normalized by the value of the first sediment trap, ST1 (Fig. 7). The inundation level parameter, $(H-h)/h$, was used to distinguish between sedimentation patterns during the peak flow development. $(H-h)/h > 1$ indicated low inundation levels (Fig. 7A) whereas $(H-h)/h \leq 1$ indicated moderate to high inundation levels (Fig. 7B). For low levels of inundation, the run-out profile of sedimentation was found during the peak flow and the peak flow drag dominated regimes for both types of vegetation, to have 4 times higher values for the coarse fraction than for the fine fraction (Fig. 7A). For high levels of inundation, the sedimentation flux of fine particles was almost constant up to the peak flow regime for both types of vegetation and decayed essentially monotonically during both the peak flow drag dominated and the gravity current regimes (Fig. 7B). The sedimentation flux of coarse particles for both types of vegetation was constant up to the mid-distances during the peak flow regime and decayed thereafter. In the later stages of flow development, during the gravity current regime,

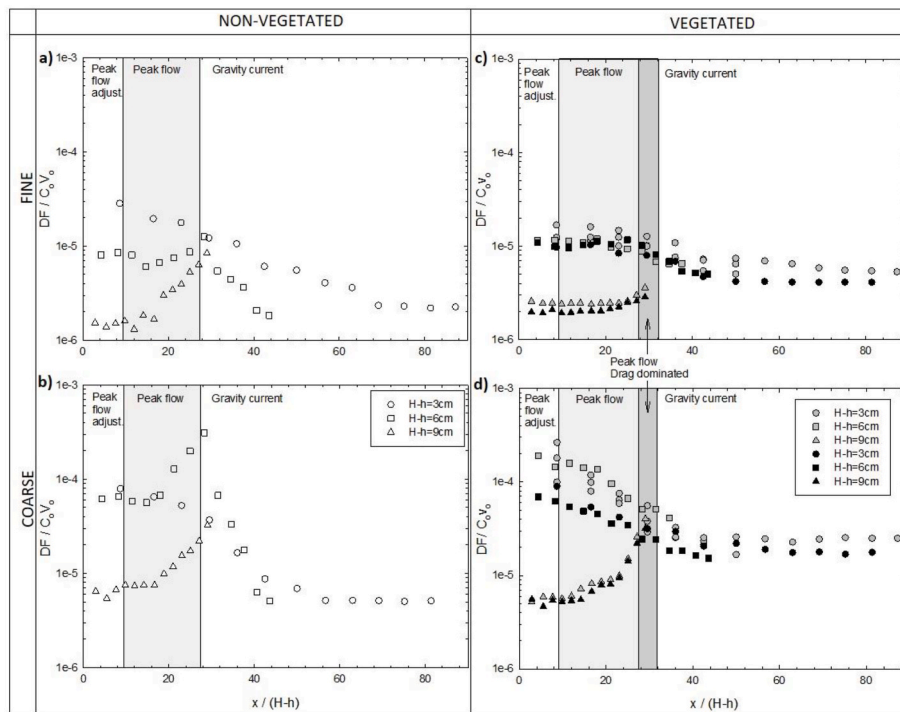


Fig. 6. Semi-logarithmic plot of the non-dimensional depositional sediment flux ($DF/C_0 \cdot v_0$) against dimensionless downstream distance ($x/(H-h)$). Left panels show results for non-vegetated experiments and right panels for vegetated experiments. Both top panels show fine sediment particles (particle diameters $< 6.2 \mu\text{m}$) and the two bottom panels coarse sediment particles ($6.2 \mu\text{m} < \text{particle diameter} < 104.0 \mu\text{m}$). All different levels on inundation, depending on $(H-h)$ values, are shown in all the graphs: $H-h = 3 \text{ cm}$ (circles), $H-h = 6 \text{ cm}$ (squares) and $H-h = 9 \text{ cm}$ (triangles). Left panel show non-vegetated experiment (with white symbols), and right panels show data for all canopies: *Juncus maritimus* (grey symbols), *Arthrocnemum fruticosum* (black symbols). The plots for non-vegetated runs are divided into three zones depending on the dynamical regime: flow adjustment, fully developed peak flow and gravity current. The plots for vegetated runs are divided into four zones depending on the dynamical regime: flow adjustment, fully developed peak flow, peak flow drag dominated and gravity current.

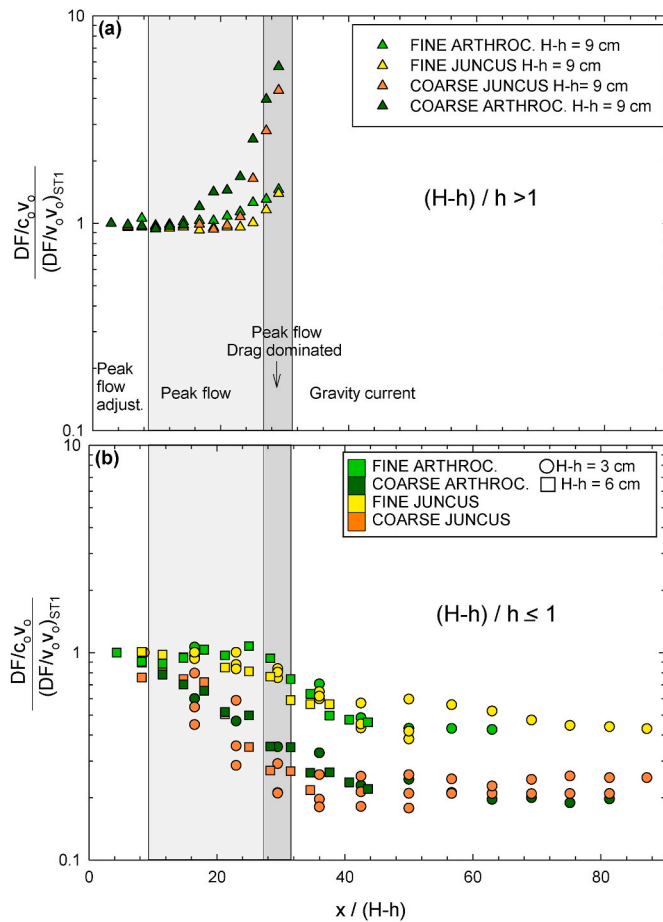


Fig. 7. Ratio of the logarithmic non-dimensional DF/C_0v_0 between the trap at x and the trap at $ST1$ plotted against dimensionless downstream distance ($x/(H-h)$) for (a) low inundated canopies $(H-h)/h > 1$, that is $H-h = 9$ cm (triangles) and (b) high inundated canopies $(H-h)/h \leq 1$, that is $H-h = 3$ cm (circles) and $H-h = 6$ cm (squares). Values are differentiated depending on particles sizes: light colours (light green and yellow) refer to fine particles (particle diameters $< 6.2 \mu\text{m}$), and dark colours (dark green and orange) to coarse particles ($6.2 \mu\text{m} < \text{particle diameter} < 104.0 \mu\text{m}$). Data for all canopies: *Juncus maritimus* (yellow and orange symbols), *Arthrocnemum fruticosum* (green symbols) are shown. The plots are divided into four zones depending on the dynamical regime: flow adjustment, fully developed peak flow, peak flow drag dominated and gravity current.

sedimentation rates in both types of vegetation were constant.

4. Discussion

Pluvial, fluvial and coastal wetlands are known to mitigate the consequences of storms exacerbated by climate change by reducing peak flows during floods. The current study mimics in the laboratory the development of peak flows in inundated wetlands. The findings reveal that a peak flow passes through four different regimes, in which the level of the inundated zone (either with vegetation or not), and the vegetated plant properties are the key parameters that control its development.

Three identified regimes were found: the peak flow-adjustment regime, the peak flow regime and the peak flow drag dominated regime (in the vegetated cases). After these initial peak flow regimes, the flow became a gravity current undergoing into the well-known drag-dominated and viscous gravity current regimes (Hatcher et al., 2000; Soler et al., 2017).

4.1. The level of inundation impacting on the hydrodynamics of peak flow

In inundated wetlands such as flooded floodplains, coastal wetlands and salt marshes, the storm magnitude (through the difference in the water level of the entering water compared to the level of the water initially inundating the wetland) is responsible for the development of the flow and the rate of sediment accretion. These results coincide with the fact that high accretion rates, driven by sedimentation in marsh zones subject to higher inundation levels, were found in the island of Sylt (Germany) after storms (Schuerch et al., 2012), or in the Nanhui tidal flat of the Changjiang Delta (China), where storms left clear signatures on tidal flat wetlands in both horizontal and vertical sedimentary features (Zhou et al., 2022).

This study has found that the level of inundation and the traits of the vegetation impact on the progression of the peak flow into the wetland canopy. For non-vegetated cases, in the initial development of the peak flow (beginning of the wetland) the velocity was dependent on $(H-h)^{1/2}$, while in the presence of vegetation the velocity was dependent on both $(H-h)^{1/2}$ and $(1-ad)$. At the beginning of the progression of the flood, the vegetation affects only the level of the effective free path it leaves (i.e. the porosity of the vegetated area, $1-ad$). That is, the greater the porosity the greater the velocity of the front of the peak flow. In contrast, at longer distances, the dependence of the progression of the peak flow front in the presence of vegetation changed to $(H-h)^{0.7}$ with vegetation affecting the peak flow development not only through the porosity, $1-ad$, but also the canopy drag, C_{Da} and also due to the level of submergence of the vegetation. The last finding would agree with Javaheri and Babbar-Sebens, 2014 who found that deep wetlands were able to minimize peak flows more than the shallow ones, reducing them up to 20% or 11%, respectively. However, to our knowledge, few studies have reported the dependence of velocities of peak flows on both the inundation level and the traits of vegetation in inundated wetlands. In this regime the velocity was a function of time, $t^{-2/5}$.

4.2. The level of inundation impacting on the sediment transport of peak flow

If the level of inundation was low, i.e., $(H-h)/h > 1$, vegetation did not control the sedimentation, with the sedimentation showing a typical run out profile during the peak flow development, with higher values during the peak flow drag regime for the coarse than for the fine particle range. Therefore, in low inundated and dry wetlands, sediments accumulate far from the source where net accumulation is expected to provoke a bed elevation. Then, in a hypothetical sequence of floods, this bed elevation may greatly reduce floodplain inundation that in turn may reduce downstream flood attenuation and increase downstream flood hazard (Guan et al., 2016). Therefore, dry wetlands would be more vulnerable in front of flooding events compared to inundated wetlands.

Besides, in low inundation conditions, and after the passage of the peak flow, the sedimentation fluxes showed that there was no segregation between the coarse and the fine fractions of sediment during the peak flow development, which for example can mediate significant amounts of sediment loads that are quickly deposited on riverbanks with sediments not being sorted hydrodynamically (Khurram et al., 2023). The lack of sorting of particle ranges, resemble flash flood partition of sediment load of arid and semiarid watersheds, in which over decades, the fluxes of the two fractions are approximately the same, with both fractions transported during small to moderate events (Malmon et al., 2004).

On the other hand, results demonstrate that marshes or wetlands with a high level of inundation, i.e., $(H-h)/h \leq 1$, could control the transport of sediments, slowing the velocity of the peak flow and enhancing their sedimentation. Therefore, a wetland can be more effective controlling the transport and deposition of sediments carried by peak flows at a critical water level. At the beginning of the peak flow development along the inundated system, there is not substantial

differential sedimentation of both fine and coarse particles with distance, but as peak flow enters in wetland canopy, and the vegetation effect increases, it is found that settling sediment is sorted by particle sizes.

High levels of inundation can strongly reduce seedling and shoot development of some plants, with some of them preferring muddy substrates to clay substrates developed at high distances (van Riel et al., 2022). Schuerch et al. (2012) identified that a critical inundation height of 18 cm in salt marshes may determine the strength of accretion. In low marsh zones subject to higher inundation levels, mean storm strength is the major factor affecting marsh accretion, whereas in high marsh zones with lower inundation levels, it is the storm frequency that impacts marsh accretion (Schuerch et al., 2012).

4.3. Wetland vegetation effect on hydrodynamics and transport of sediments

Our study has demonstrated that the presence of vegetation decreases the level of inundation needed for the system to be effective in enhancing the settling of sediment transported by the peak flow. Run out sedimentation profiles were observed for low inundation levels, which were enhanced by the presence of vegetation for both the fine and coarse particle fractions. In the initial stages of the peak flow, vegetation also modified the hydrodynamics of the peak flow, reducing the peak flow velocity as the vegetation porosity decreased. At later stages, the modification was determined to be a function of both vegetation porosity and the drag coefficient.

Modification of peak flow velocity can be seen with the ratio between the non-dimensional velocity travelled by a peak flow event through a non-vegetated area (Eq. (5)) and that travelled over a vegetated areas (Eq. (7)):

$$\frac{v_{veg}}{v_{non-veg}} = 0.68 \cdot (1 - ad) \quad (10)$$

Velocity in vegetated wetlands reduces directly proportional to the frontal area of plants stems per unit volume (ad), that means that not only the vegetation density but also the morphologic characteristics of plants (with more or less leaves, thinner or wider stems, ...) have to be considered in order to know the level of reduction in velocity peak flow. Wetland plant community and abundance of species will vary over time, as well as plants morphology. These changes will happen along the year (seasonal), impacting on the reduction on peak flow velocity by the wetland. Kadlec (1990) claimed that natural vegetation ranges between $ad = 0.01$ and 0.1 which corresponds to a range from 83 to 826 plants/m² for *J. maritimus*, or from 39 to 391 plants/m² for *A. fruticosum* (natural plants taken for performing the experiments). Therefore, depending on the vegetation morphology, wetlands could reduce the velocity from 32% to 39% (corresponding to thicker and thinner plant stems, respectively).

Vegetation not only has an effect on velocity but also in the distance reached by the peak flow once enters in the wetland. Therefore, as found in equation (10) this study demonstrates that the ratio between the non-dimensional distance travelled by a peak flow event through a non-vegetated area (Eq. (4)) and that travelled over a vegetated areas (Eq. (6)), is

$$\frac{\left(\frac{x}{H-h}\right)_{veg}}{\left(\frac{x}{H-h}\right)_{non-veg}} = 0.68 \cdot (1 - ad) \quad (11)$$

indicating that for canopies with a greater frontal area of plants, peak flow arrives a 20% further than for non-vegetated wetlands.

However, once a wetland is vegetated, the density of vegetation plays a minor role. For example, comparing the densest to the sparsest canopies that can be found in natural vegetation (which following Kadlec (1990), and taking a typical wetland plant as *Spartina alterniflora*,

would correspond to 69 to 694 plants/m²), it results in,

$$\frac{\left(\frac{x}{H-h}\right)_{veg,ad=0.1}}{\left(\frac{x}{H-h}\right)_{veg,ad=0.1}} = (1 - ad)^{0.22} = 0.98, \quad (12)$$

which means that denser canopies only reduce by a 2% the extension reached by the peak flow flowing through sparser canopies.

From equation for the distance travelled by a peak flow event over a vegetated area (see Eq. (8)):

$$x_{veg} = 13.8 \left(g^{T^2}\right)^{0.3} \cdot (H - h)^{0.7} \cdot (C_{Da}(1 - ad))^{0.22} \quad (13)$$

the first term on the right-hand side can be related to the effect of the submergence level of the vegetated stems, whereas the second can be attributed to the effect of both the drag and the density of the vegetation. Considering the effect on the peak flow entrance of high inundated vegetated wetlands to low inundated vegetated wetlands ($H-h = 9$ and 3 cm respectively) it is found a ratio $(x)_{INUNDATED}/(x)_{NON-INUNDATED}$ of 0.46 . This result indicates that the presence of vegetation reduces the extension of the peak flow to approximately half its value for the non-inundated case. This result is in accordance with Fairchild et al. (2021) who found a reduction in the flooded area of ~ 0.46 for low storm magnitudes and 0.68 for high storm magnitudes. As well as with studies realized by De Laney (1995) that found a reduction in peak flow due to construction of wetlands concluding that 5%–10% of the wetlands area in the watershed could attenuate around 50% of peak floods, and a little bit greater than the 42% found in Eagle Creek watershed (Indiana, USA) (Javaheri and Babbar Sebens, 2014).

In addition, the current study demonstrates that the higher the peak flow magnitude (i.e., $H-h$), the higher the ratio $(x/(H-h))_{veg}/(x/(H-h))_{non-veg}$. This result indicates that vegetation has a smaller capacity to attenuate deeper flooding events than shallower ones.

In the peak flow drag dominated regime, the reduction of velocity along with the increased sediment deposition depended on the vegetation. The higher frontal area of *A. fruticosum* could induce lower sedimentation of coarser particles associated with higher flow velocities through the vegetation (Serra et al., 2017, 2021). For high inundation levels, at shorter distances of flow development the coarse and fine sediment did not show differential settling with distance. At intermediate and large distances, the sedimentation profile with distance presented a monotonically decreasing development that was not affected by the type of vegetation, with the sedimentation of fine particles being higher than the sedimentation of coarse particles. This process has also been identified in the sedimentation of particles in gravity currents, and is known as the “muddification” process, in which the presence of fine particles in deposited sediments is higher (Soler et al., 2020).

4.4. Wetland control on floodings

In the ephemeral and dry channels, the development of a high peak flow can be very hazardous and damaging, with many reported inundation events, resulting in large amounts of sediment mobilisation and high rates of sedimentation (Camarasa-Belmonte, 2016; Hooke, 2019). The characteristics of these ephemeral channels are the lack of channel bed armour, high sediment supply, and equal mobility of sediment sizes. Due to climate change, wetlands will experience drought cycles more frequent and severe in the future (Middleton and Kleinebecker, 2012), that will become in a reduction of vegetation (Jenkins and Boulton, 2007). Consequently, wetlands will become more vulnerable to flood events. Studies carried out by Longobardi et al. (2003) across different countries (Australia, New Zealand and Italy) have shown that the ratio between the quick peak flow and the rainfall volume (run off coefficient) is dependent on the soil moisture prior to the event, anticipating higher peak flows and associated floodings for dryer wetlands. But not only this, sedimentation patterns are expected to differ between dry and

inundated wetlands. Therefore, the future fate of the bed elevation and morphometry will also change differently in front of the inundation level after facing a flooding event.

Vegetation, through the vegetation porosity and canopy drag, altered the hydrodynamical development of the peak flow and the associated transport and sediment depositional patterns. The results regarding both peak flow development and sediment transport showed that the hydrodynamic, morphodynamic and ecological processes in floodplains, coastal wetlands and marshes may present both spatial and evolutionary characteristics that are governed by both the traits of the vegetation and the level of inundation in the system, at short time scales (Guan et al., 2016; Tsoi et al., 2022). Among all wetland services, flood control and climate change mitigation are the most important services for the human communities (Mitsch and Gosselink, 2007) so it is necessary to know the critical water level of inundated systems at which coastal wetland systems, can sustain most of its services.

In the period of 1998–2017 floods affected more than 2 billion people (UNISDR, 2018) causing considerable economic losses that can increase due to the anthropogenic warming. For example, for a mean global air temperature increase of 1.5 °C, and depending on the socio-economic scenario, human losses from flooding could rise by 70–83% (Dottori et al., 2018). Therefore, it might be of great interest understanding the hydrological services provided by wetlands to face these future scenarios as they have great potential to be used as nature-based solutions for regulation of pluvial, fluvial or coastal floodings (Rojas et al., 2022). Therefore, conservation practices in wetlands should be fuelled to fight against peak flows in coastal areas. Results found show that densest vegetated wetlands would be very effective in reducing the circulation of a peak flow, not only by reducing the velocity between a 35 or 39% but also reducing a 20% the peak flow fetch within the wetland. Furthermore, inundated wetlands are expected to be even more effective than dry wetlands, raising the protection benefits of a wetland to a 50%.

5. Conclusion

Under flooding processes, inundated systems with vegetation may or may not control the hydrodynamics and sediment deposition with distance depending on the strength of the flooding event. In this study, the development of particle-laden peak flow has been studied in systems that can be subject to both low and high inundation conditions. The longitudinal evolution of the peak flow front was characterized by three temporal regimes: firstly, the peak flow-adjustment regime, then the established peak flow regime, and finally the peak flow drag dominated regime. At larger distances, the flow developed into a gravity current and evolved further through drag-dominated and viscous gravity current regimes. Sediment transport and depositional flux rates associated to the flooding event presented patterns that depended also on the inundation level. High inundations were able to transport sediment particles inland into the marsh whereas in low inundation levels the sedimentation was greater close to the source decreasing progressively into the marsh. Vegetation affected the peak flow in its early stages only by reducing the cross-section of the flow but keeping the non-dimensional flow velocity constant. However, as the peak flow developed further, the plants produced drag forces on the flow in the peak flow drag regime where the velocity of the flow decreased with time.

To summarise, this study investigated the hydrodynamics and sediment deposition during the beginning of flooding events (peak flow) and reports the variation of velocity with distance, finding it to depend on inundation levels, reduced gravity, vegetation porosity, vegetation drag, and time. It also investigated the longitudinal profile of sediment deposition under low and high inundation levels in the presence of vegetation. The results may help to understand the impacts of extreme pluvial, fluvial and coastal flooding events in vegetated floodplains, and wetlands, and can be applied to coastal wetland flood risk management with the purpose of mitigating and fighting against peak flows.

CRedit authorship contribution statement

Marianna Soler: Writing – review & editing, Writing – original draft, Methodology, Formal analysis, Data curation, Conceptualization. **Jordi Colomer:** Writing – review & editing, Formal analysis, Data curation, Conceptualization. **Andrew Folkard:** Writing – review & editing, Data curation. **Teresa Serra:** Writing – review & editing, Supervision, Funding acquisition, Conceptualization.

Declaration of competing interest

The authors declare that they have no known competing financial interests or personal relationships that could have appeared to influence the work reported in this paper.

Data availability

Data will be made available on request.

Acknowledgments

This work was supported by the Ministerio de Ciencia e Innovación of the Spanish Government [PID 2021-12386003-100].

Open Access funding provided thanks to the CRUE-CSIC agreement with Elsevier.

Appendix A. Supplementary data

Supplementary data to this article can be found online at <https://doi.org/10.1016/j.marenvres.2024.106669>.

References

- Acreman, M., Holden, J., 2013. How wetlands affect floods. *Wetlands* 33 (5), 773–786. <https://doi.org/10.1007/s13157-013-0473-2>.
- Babbar-Sebens, M., Barr, R.C., Tedesco, L.P., Anderson, M., 2013. Spatial identification and optimization of upland wetlands in agricultural watersheds. *Ecol. Eng.* 52, 130–142. <https://doi.org/10.1016/j.ecoleng.2012.12.085>.
- Balwan, W.K., Kour, S., 2021. Wetland-an ecological boon for the environment. *African Scholars J. Agri. Life Sci.* 4 (3), 38–48. <https://doi.org/10.13140/RG.2.2.15728.79368>.
- Barcelona, A., Serra, T., Colomer, J., 2018. Fragmented canopies control the regimes of gravity currents development. *J. Geophys. Res-Oceans* 123. <https://doi.org/10.1002/2017JC01314>.
- Bouma, T.J., Olenin, S., Reise, K., Ysebaert, T., 2009. Ecosystem engineering and biodiversity in coastal sediments: posing hypotheses. *Helgol. Mar. Res.* 63, 95–106. <https://doi.org/10.1007/s10152-009-0146-y>.
- Brémond, P., Grelot, F., Agenais, A.L., 2013. Review article: economic evaluation of flood damage to agriculture – review and analysis of existing methods. *Nat. Hazards Earth Syst. Sci.* 13 (10), 2493–2512. <https://doi.org/10.5194/nhess-13-2493-2013>.
- Camarasa-Belmonte, M., 2016. Flash floods in mediterranean ephemeral streams in valencia region (Spain). *J. Hydrol.* 541 (A), 99–115. <https://doi.org/10.1016/j.jhydrol.2016.03.019>.
- Casanova, M.T., Brock, M.A., 2000. How do depth, duration and frequency of flooding influence the establishment of wetland plant communities? *Plant Ecol.* 147 (2), 237–250, 2000.
- Chen, Y., Rasool, M.A., Hussain, S., Meng, S., Yao, Y., Wang, X., Liu, Y., 2023. Bird community structure is driven by urbanization level, blue-green infrastructure configuration and precision farming in Taizhou. *China. Sci. Total Environ.* 859, 160096 <https://doi.org/10.1016/j.scitotenv.2022.160096>.
- Choi, S.M., Seo, J.Y., Jeong, S.W., Lee, M.J., Ha, H.K., 2021. Disturbance of sedimentary processes in tidal salt marshes invaded by exotic vegetation. *Sci. Total Environ.* 799, 149393 <https://doi.org/10.1016/j.scitotenv.2021.149393>.
- Dakhalla, A.O., Parajuli, P.B., 2016. Evaluation of the best management practices at the watershed scale to attenuate peak streamflow under climate change scenarios. *Water Resour. Manag.* 30 (3), 963–982. <https://doi.org/10.1007/s11269-015-1202-9>.
- Davidson, C.N., 2014. How much wetland has the world lost? Long term and recent trends in global wetland area. *Mar. Freshw. Res.* 65, 934–941. <https://doi.org/10.1071/MF14173>.
- De Laney, T.A., 1995. Benefits to downstream flood attenuation and water quality as a result of constructed wetlands in agricultural landscapes. *J. Soil Water Conserv.* 50 (6), 620–626.
- Dottori, F., Szweczyk, W., Ciscar, J.C., et al., 2018. Increased human and economic losses from river flooding with anthropogenic warming. *Nat. Clim. Change* 8, 781–786. <https://doi.org/10.1038/s41558-018-0257-z>.

- Duarte, C.M., 2002. The future of seagrass meadows. *Environ. Conserv.* 29, 192–206. <https://doi.org/10.1017/S0376892902000127>.
- Fairchild, T.P., Bennett, W.G., Smith, G., Day, B., Skov, M.W., Möller, I., Beaumont, N., Karunaratna, H., Griffin, J.N., 2021. Coastal wetlands mitigate storm flooding and associated costs in estuaries. *Environ. Res. Lett.* 16, 074034 <https://doi.org/10.1088/1748-9326/ac0c45>.
- Faulkner, S., Barrow, W., Keeland, B., Walls, S., Telesco, D., 2011. Effects of conservation practices on wetland ecosystem services in the Mississippi Alluvial Valley. *Ecol. Appl.* 21 (3), S31–S48. <https://doi.org/10.1890/10-0592.1>.
- Ferreira, C.S.S., Kasanin-Grubin, M., Kapovi, M., Solomun, Sushkova, S., Minkina, T., Zhao, W., Kalantari, Z., 2023. Wetlands as nature-based solutions for water management in different environments. *Current Opinion in Environmental Science & Health* 33, 100476. <https://doi.org/10.1016/j.coesh.2023.100476>, 2023.
- Fu, H., Xu, J., Zhang, H., García Molinos, J., Zhang, M., Klaar, M., Broen, L.E., 2023. A meta-analysis of environmental responses to freshwater ecosystem restoration in China (1987–2018). *Environ. Pollut.* 316, 120589 <https://doi.org/10.1016/j.envpol.2022.120589>.
- Gardner, R.C., Finlayson, M., 2018. Ramsar convention on wetlands. (2018). Global wetland outlook: state of the world's wetlands and their services to people. Gland, Switzerland: ramsar. Convention Secretariat.
- Gedan, K.B., Silliman, B.R., Bertness, M.D., 2009. Centuries of human-driven change in salt marsh ecosystems. *Ann. Rev. Mar. Sci.* 1, 117–141. <https://doi.org/10.1146/annurev.marine.010908.163930>.
- Ghisalberti, M., Nepf, H.M., 2004. The limited growth of vegetated shear layers. *Water Resour. Res.* 40, W07502 <https://doi.org/10.1029/2003WR002776>.
- Guan, M., Carrivick, J.L., Wright, N.G., Sleight, P.A., Staines, K.E., 2016. Quantifying the combined effects of multiple extreme floods on river channel geometry and on flood hazards. *J. Hydrol.* 538, 256–268. <https://doi.org/10.1016/j.jhydrol.2016.04.004>.
- Hatcher, L., Hogg, A.J., Woods, A.W., 2000. The effect of drag on turbulent gravity currents. *J. Fluid Mech.* 416, 297–314.
- Healy, M.G., Siggins, A., Molloy, K., Potito, A.P., O'Leary, D., Daly, E., Callery, O., 2023. The impact of alternating drainage and inundation cycles on geochemistry and microbiology of intact peat cores. *Sci. Total Environ.* 858, 159664 <https://doi.org/10.1016/j.scitotenv.2022.159664>.
- Hoggart, S.P.G., Hanley, M.E., Parker, D.J., Simmonds, D.J., Bilton, D.T., Filipova-Marinova, M., Franklin, E.L., Kotsev, I., Penning-Rowsel, E.C., Rundle, S.D., Trifonova, E., Vergiev, S., White, A.C., Thompson, R.C., 2014. The consequences of doing nothing: the effects of seawater flooding on coastal zones. *Coast. Eng.* 87, 169–182. <https://doi.org/10.1016/j.coastaleng.2013.12.001>.
- Hooke, J.M., 2019. Extreme sediment fluxes in a dryland flash flood. *Sci. Rep.* 9 (1), 1686. <https://doi.org/10.1038/s41598-019-38537-3>.
- Javaheri, A., Babbar-Sebens, M., 2014. On comparison of peak flow reductions, flood inundation maps, and velocity maps in evaluating effects of restored wetlands on channel flooding. *Ecol. Eng.* 73, 132–145. <https://doi.org/10.1016/j.ecoleng.2014.09.021>.
- Jenkins, K.M., Boulton, A.J., 2007. Detecting impacts and setting restoration targets in riparian zones: aquatic micro-invertebrate responses to reduced floodplain inundation. *J. Appl. Ecol.* 44, 823–832. <https://doi.org/10.1111/j.1365-2664.2007.01298.x>.
- Jessop, J., Spyreas, G., Pociask, G.E., Benson, T.J., Ward, M.P., Kent, A.D., Matthews, J. W., 2015. Tradeoffs among ecosystem services in restored wetlands. *Biol. Conserv.* 191, 341–348. <https://doi.org/10.1016/j.biocon.2015.07.006>.
- Jones, H.P., Nickel, B., Srebotnjak, T., Turner, W., Gonzalez-Roglich, M., Zavaleta, E., Hole, D.G., 2020. Global hotspots for coastal ecosystem-based adaptation. *PLoS One* 15 (5), e02333005. <https://doi.org/10.1371/journal.pone.0233305>.
- Junk, W.J., An, S., Finlayson, C.M., Gopal, B., Květ, J., Mitchell, S.A., Mitsch, W.J., Roberts, R.D., 2013. Current state of knowledge regarding the world's wetlands and their future under global climate change: a synthesis. *Aquat. Sci.* 75, 151–167. <https://doi.org/10.1007/s00027-012-0278-z>.
- Kadlec, R.H., 1990. Overland flow in wetlands: vegetation resistance. *J. Hydraul. Eng.* 116 (5), 691–706.
- Khurram, D., Bao, Y., Tang, Q., He, X., Li, J., de, D., Nambajimana, J., Nsibirmana, G., 2023. Sedimentary geochemistry mediated by specific hydrological regime in the water level fluctuation zone of the Three Gorges Reservoir, China. *Environ. Sci. Pollut. Res.* 10.1007/s11356-022-25086-y.
- Kundzewicz, Z.W., Pinskiar, I., 2022. Are pluvial and fluvial floods on the rise? *Water* 2022 14, 2612. <https://doi.org/10.3390/w14172612>.
- Laronne, J., Reid, I., 1993. Very high rates of bedload sediment transport by ephemeral desert rivers. *Nature* 366, 148–150. <https://doi.org/10.1038/366148a0>.
- Larson, J.S., Adamus, P.R., 1989. *Functional Assessment of Freshwater Wetlands: A Manual and Training Outline, No. 89*. University of Massachusetts, at Amherst.
- Lefebvre, G., Redmond, L., Germain, C., Palazzi, E., Terzagio, S., Willm, L., Poulin, B., 2019. Predicting the vulnerability of seasonally-flooded wetlands to climate change across the Mediterranean Basin. *Sci. Total Environ.* 692, 546–555. <https://doi.org/10.1016/j.scitotenv.2019.07.263>.
- Lemke, D., Richmond, S., 2009. Iowa drainage and wetlands landscape systems initiative. Farm Foundation Report. <http://www.farmfoundation.org/news/articlefiles/1718-LemkeandRichmond.pdf>.
- Leonard, L.A., Luther, M.A., 1995. Flow hydrodynamics in tidal marsh canopies. *Limnol. Oceanogr.* 40 (8), 1474–1484.
- Lo, V.B., Bouma, T.J., van Belzen, J., Van Colen, C., Airolidi, L., 2017. Interactive effects of vegetation and sediment properties on erosion of salt marshes in the Northern Adriatic Sea. *Mar. Environ. Res.* 131, 32–42. <https://doi.org/10.1016/j.marenvres.2017.09.006>.
- Longobardi, A., Villani, P., Grayson, R.B., Western, A.W., 2003. On the relationship between runoff coefficient and catchment initial conditions. In: *Proceedings of MODSIM*, pp. 867–872.
- Luo, C., Fu, X., Zeng, X., Cao, H., Wang, J., Ni, H., Qu, Y., Liu, Y., 2022. Responses of remnant wetlands in the Sanjiang Plain to farming-landscape patterns. *Ecol. Indic.* 135, 108542 <https://doi.org/10.1016/j.ecolind.2022.108542>.
- Malmton, D.V., Reneau, S.L., Dunne, T., 2004. Sediment sorting and transport by flash floods. *J. Geophys. Res.* 109, F02005 <https://doi.org/10.1019/2003JF000067>.
- Marbà, N., Duarte, C.M., 2010. Mediterranean warming triggers seagrass (*Posidonia oceanica*) shoot mortality. *Global Change Biol.* 16, 2366–2375 <https://doi.org/10.1111/j.1365-2486.2009.02130.x>.
- McGrath, G., Harding, C., Matte, P., 2023. Changing processes flooding a salt marsh in a microtidal estuary with a drying climate. *Estuar. Coast Shelf Sci.* 296, 108573 <https://doi.org/10.1016/j.ecss.2023.108573>.
- Middleton, B.A., Kleinebecker, T., 2012. The effects of climate-change-induced drought and freshwater wetlands. In: Middleton, B. (Ed.), *Global Change and the Function and Distribution of Wetlands*, Global Change Ecology and Wetlands, vol. 1. Springer, Dordrecht. https://doi.org/10.1007/978-94-007-4494-3_4.
- Mitsch, W.J., Day, J.W., 2006. Restoration of wetlands in the Mississippi-Ohio-Missouri (MOM) river basin: experience and needed research. *Ecol. Eng.* 26, 55–69.
- Mitsch, W.J., Gosselink, J.G., 2007. *Wetlands*, fourth ed. John Wiley & Sons, Inc., Hoboken, USA.
- Montakhab, A., Yusuf, B., Ghazali, A.H., Mohamed, T.A., 2012. Flow and sediment transport in vegetated waterways: a review. *Rev. Environ. Sci. Biotechnol.* 11 (3), 275–287. <https://doi.org/10.1007/s11157-012-9266-y>.
- Nahlik, A., Fennessy, M., 2016. Carbon storage in US wetlands. *Nat. Commun.* 7, 13835 <https://doi.org/10.1038/ncomms13835>.
- Nepf, H.M., 1999. Drag, turbulence, and diffusion in flow through emergent vegetation. *Water Resour. Res.* 35 (2), 479–489.
- Pattison-Williams, J.K., Pomeroy, J.W., Badiou, P., Gabor, S., 2018. Wetlands, flood control and ecosystem services in the smith Creek drainage basin: a case study in saskatchewan, Canada. *Ecol. Econ.* 147, 36–47. <https://doi.org/10.1016/j.ecolecon.2017.12.026>.
- Pujol, D., Colomer, J., Serra, T., Casamitjana, X., 2010. Effect of submerged aquatic vegetation on turbulence induced by an oscillating grid. *Contin. Shelf Res.* 30, 1019–1029. <https://doi.org/10.1016/j.csr.2010.02.014>.
- Pujol, D., Serra, T., Colomer, J., Casamitjana, X., 2013. Flow structure in canopy models dominated by progressive waves. *J. Hydrol.* 486, 281–292. <https://doi.org/10.1016/j.jhydrol.2013.01.024>.
- Reed, D., van Wesenbeeck, B., Herman, P.M.J., Meselhe, E., 2018. Tidal flat-systems as flood defences: understanding biogeomorphic controls. *Estuar. Coast Shelf Sci.* 213, 269–282. <https://doi.org/10.1016/j.ecss.2018.08.017>.
- Rojas, O., Soto, E., Rojas, C., López, J.J., 2022. Assessment of the flood mitigation ecosystem service in a coastal wetland and potential impact of future urban development in Chile. *Habitat Int.* 123, 102554 <https://doi.org/10.1016/j.habitatint.2022.102554>.
- Sauer, J., 2022. *Pluvial Flood Risk Modelling, Assessment, and Management under Evolving Urban Climates and Land Cover*. Arizona State University, Thesis.
- Schuerch, M., Rapaglia, J., Liebetrau, V., Vafeidis, A., Reise, K., 2012. Salt marsh accretion and storm tide variation: an example from a barrier island in the North Sea. *Estuar. Coast* 34, 486–500. <https://doi.org/10.1007/s12237-011-9461-z>.
- Serra, T., Ros, A., Vergés, C., Casamitjana, X., 2017. Influence of a flooding event discharge on accretion in wetlands. *Environ. Fluid Mech.* 17, 833–851. <https://doi.org/10.1007/s10652-017-9528-x>.
- Serra, T., Font, E., Soler, M., Barcelona, A., Colomer, J., 2021. Mean residence time of lagoons in shallow vegetated floodplains. *Hydrol. Process.* 35, e14065 <https://doi.org/10.1002/hyp.14065>.
- Sheng, P.Y., Paramygin, V.A., Rivera-Nieves, A.A., Ruizhi, Z., Fernald, S., Hall, T., Jacob, K., 2022. Coastal marshes provide valuable protection for coastal communities from storm-induced wave, flood, and structural loss in a changing climate. *Sci. Rep.* 12 (1), 3051. <https://doi.org/10.1038/s41598-022-06850-z>.
- Shin, W., Oh, M., Hong, J.-S., Byun, C., Lee, E.J., 2022. Early invasion of common cordgrass (*Spartina anglica*) increases belowground biomass and decreases macrofaunal density and diversity in a tidal flat marsh. *Biol. Invasions* 24 (11), 3615–3629. <https://doi.org/10.1007/s10530-022-02866-8>.
- Soler, M., Colomer, J., Serra, T., Casamitjana, X., Folkard, A.M., 2017. Sediment deposition from turbidity currents in simulated aquatic vegetation canopies. *Sedimentology* 64, 1132–1146. <https://doi.org/10.1111/sed.12342>.
- Soler, M., Colomer, J., Folkard, A., Serra, T., 2020. Particle size segregation of turbidity current deposits in vegetated canopies. *Sci. Total Environ.* 703, 134784 <https://doi.org/10.1016/j.scitotenv.2019.134784>.
- Soler, M., Serra, T., Folkard, A., Colomer, J., 2021. Hydrodynamics and sediment deposition in turbidity currents: comparing continuous and patchy vegetation canopies, and the effects of water depth. *J. Hydrol.* 594, 125750 <https://doi.org/10.1016/j.jhydrol.2020.125750>.
- Tsoi, W., Grouns, I., Southwell, M., Mika, S., Lewis, S., Ryder, D., Frazier, P., 2022. Effects of inundation on water quality and invertebrates in semiarid floodplain wetlands. *Inland Waters* 12 (3), 397–407. <https://doi.org/10.1080/20442041.2022.2057164>.
- UNISDR, C., 2018. *Economic Losses, Poverty, & Disasters 1998-2017*. CRED-UNISDR.
- Van Riel, M.C., Vonk, J.A., Verdonschot, R.C.M., Muñoz, J.F., Verdonschot, P.F.M., 2022. Using dredged sediments to support wetland plant development in a constructed delta lake. *Ecol. Eng.* 178, 106568 <https://doi.org/10.1016/j.ecoleng.2022.106568>.
- Wamsley, T.V., Cialone, M.A., Smith, J.M., Atkinson, J.H., Rosati, J.D., 2010. The potential of wetlands in reducing storm surge. *Ocean Eng.* 37 (1), 59–68. <https://doi.org/10.1016/j.oceaneng.2009.07.018>. ISSN 0029-8018.
- White, F.M., 1991. *Viscous Fluids Flow*, second ed. McGraw-Hill, New York.
- Zhou, Z., Wu, Y., Fan, D., Wu, G., Luo, F., Yao, P., Gong, Z., Coco, G., 2022. Sediment sorting and bedding dynamics of tidal flat wetlands: modeling the signature of storms. *J. Hydrol.* 610, 127913 <https://doi.org/10.1016/j.jhydrol.2022.127913>.